Molecular fingerprints of star formation throughout the Universe : a space-based infrared study

Lahuis, F.

Chapter 8

Infrared Molecular Starburst Fingerprints in Deeply Obscured (Ultra)Luminous Infrared Galaxy Nuclei

Abstract

High-resolution spectra of the *Spitzer* Space Telescope show vibration-rotation absorption bands of gaseous C_2H_2, HCN, and CO_2 molecules toward a sample of deeply obscured (U)LIRG nuclei. The observed bands reveal the presence of dense ($n \gtrsim 10^7\,\mathrm{cm}^{-3}$), warm ($T_{\rm ex} = 200 - 700\,\mathrm{K}$) molecular gas with high column densities of these molecules ranging from a few 10^{15} to $10^{17}\,\mathrm{cm}^{-2}$. Abundances relative to H_2, inferred from the silicate optical depth, range from $\sim 10^{-7}$ to 10^{-6} and show no correlation with temperature. Theoretical studies show that the high abundances of both C_2H_2 and HCN exclude an X-ray dominated region (XDR) associated with the toroid surrounding an AGN as the origin of this dense warm molecular gas. Galactic massive protostars in the so-called hot-core phase have similar physical characteristics with comparable high abundances of C_2H_2, HCN, and CO_2 in the hot phase. However, the abundances of C_2H_2 and HCN and the C_2H_2/CO_2 and HCN/CO_2 ratios are much higher toward the (U)LIRGs in the cooler ($T_{\rm ex} \lesssim 400\,\mathrm{K}$) phase. We suggest that the warm dense molecular gas revealed by the mid-IR absorption lines is associated with a phase of deeply embedded star formation, where the extreme pressures and densities of the nuclear starburst environment have inhibited the expansion of H II regions and the global disruption of the star-forming molecular cloud cores, and have 'trapped' the star formation process in an 'extended' hot-core phase.

Lahuis, F., Spoon, H. W. W., Tielens, A. G. G. M., Doty, S. D., Armus, L., Charmandaris, V., Houck, J. R., Stäuber, P., & van Dishoeck, E. F. 2007, ApJ, 659, 296

8.1 Introduction

One of the holy grails in the study of luminous and ultraluminous infrared galaxies (LIRGs and ULIRGs) is to elucidate the true nature of the central energy source. (U)LIRGs emit nearly all their energy in the mid- and far-infrared part of the spectrum. LIRGs have a luminosity $L_{8-1000\mu\mathrm{m}} > 10^{10} L_{\odot}$ and ULIRGs $L_{8-1000\mu\mathrm{m}} > 10^{12} L_{\odot}$, equal to the power output of quasars. (U)LIRGs are generally found in interacting and merging systems (e.g, Armus et al., 1987; Sanders et al., 1988b; Murphy et al., 1996). During the merger large amounts of gas and dust are concentrated toward the nucleus (e.g., Mihos & Hernquist, 1996), fueling a massive starburst and possibly a massive black hole (an AGN). (U)LIRGs are without doubt the most spectacular sites of star formation in the Universe, and if a substantial part of their energy originates from AGN activity, it would show the AGN in its very earliest deeply enshrouded phase.

The sensitive Infrared Spectrograph (IRS, Houck et al., 2004) on board the *Spitzer* Space Telescope (Werner et al., 2004) has revealed the richness, complexity, and diversity of the mid-infrared spectra toward a sample of deeply obscured (U)LIRGs (Armus et al., 2004, 2006, 2007; Spoon et al., 2005, 2006); see Genzel & Cesarsky (2000) for a review of results from the Infrared Space Observatory (ISO). The general characteristic of these spectra is the presence of deep, broad absorption of amorphous silicates, centered at 10 and 18 μm. In addition, the spectra show a large variety in absorption features of crystalline silicates, aliphatic hydrocarbons, water ice, and gas phase bands of hot CO (Spoon et al., 2004, 2007). Polycyclic aromatic hydrocarbons (PAH) emission bands are generally weak and in some cases absent. Absorption bands of more volatile ices (e.g. CO or CO_2), commonly detected in Galactic dense molecular clouds, are generally absent or very weak.

The very compact nuclei of deeply obscured (U)LIRGs are packed with gas. Molecular gas has been observed at millimeter wavelengths, through its low-lying pure rotational transitions, in (U)LIRG nuclei (e.g., Solomon et al., 1997; Downes & Solomon, 1998), see Aalto (2005) for a recent overview. In recent years millimeter emission lines of HCN and HCO^+ have been observed revealing the presence of relatively dense ($n_{\mathrm{H}} \sim 10^5\,\mathrm{cm}^{-3}$) molecular gas (Imanishi et al., 2006; Kohno, 2005). However, the analysis of the millimeter emission lines is complicated as a result of beam dilution, which strongly depends on the molecules and transitions observed.

The IRS Short-High spectrometer (IRS-SH) on board the *Spitzer* Space Telescope allows, for the first time, the direct study of the very dense and warm molecular gas in the central regions of deeply obscured luminous and ultraluminous infrared galaxies through IR pencil-beam line-of-sight absorption spectroscopy against the continuum of individual nuclei or unresolved[1] double nuclei. In particular, the mid-infrared vibration-rotation bands of C_2H_2 and HCN uniquely trace warm ($100 < T < 1000\,\mathrm{K}$) and dense ($n_{\mathrm{H}} > 10^7\,\mathrm{cm}^{-3}$) molecular gas. These bands have previously been detected primarily toward Galactic massive protostars (Lacy et al., 1989; Evans et al., 1991; Lahuis & van Dishoeck, 2000). They may prove to be a new strong tool to probe the heating sources of deeply obscured (U)LIRG nuclei (starburst or AGN activity).

[1] The IRS SH slit width is $4.7''$, equal to the size of the point-spread function at $19.5\,\mu$m.

Table 8.1. Observation details and basic source properties

Target	AOR key	Pipeline	Observed	Int. time[a] (sec)	z	$\log \frac{L_{\rm IR}}{(L_\odot)}$	$\tau_{9.7}$	Opt./NIR[b] Class	D_L[c] (Mpc)
IRAS 17208-0014	4986624	S12.0.2	2004 Mar 27	$31 \times 6 \times 2$	0.0430	12.46	1.9	H II	188
Arp 220	4983808	S12.0.2	2004 Feb 29	$31 \times 6 \times 2$	0.0181	12.17	3.3	LINER[1]	78
IC 860	6652416	S13.2.0	2005 Feb 10	$121 \times 2 \times 2$	0.0112	10.96	2.1		48
IRAS 22491-1808	4990976	S13.2.0	2004 Jun 24	$121 \times 2 \times 2$	0.0773	12.19	1.1	Starburst[2,3]	346
NGC 4418	4935168	S13.2.0	2005 Jul 8	$31 \times 6 \times 2$	0.0073	11.03	4.4		31
IRAS 13218+0552	4979200	S13.2.0	2004 Jul 17	$121 \times 3 \times 2$	0.2051	12.71	0.8	QSO/Sey-1[4,5]	998
IRAS 15250+3609	4983040	S12.0.2	2004 Mar 4	$31 \times 6 \times 2$	0.0554	12.05	3.8		244
IRAS 05189-2524	4969216	S13.2.0	2004 Mar 22	$31 \times 6 \times 2$	0.0426	12.19	0.4	Seyfert-2/1[6]	186
Mrk 231	4978688	S13.2.0	2004 Apr 14	$31 \times 6 \times 2$	0.0422	12.52	0.8	Seyfert-1[2]	184
Mrk 273	4980224	S12.0.2	2004 Apr 14	$31 \times 6 \times 2$	0.0378	12.15	1.9	Seyfert-2	164
IRAS 00397-1312	4963584	S12.0.2	2004 Jan 4	$121 \times 3 \times 2$	0.2617	12.90	3.3		1317
IRAS 20100-4156	4989696	S13.2.0	2004 Apr 13	$121 \times 2 \times 2$	0.1296	12.65	3.3		601
UGC 5101	4973056	S13.2.0	2004 Mar 23	$31 \times 6 \times 2$	0.0400	12.00	1.7	LINER[3]	164
IRAS 01003-2238	4972032	S12.0.2	2004 Jan 4	$121 \times 2 \times 2$	0.1177	12.29	0.7		542
IRAS 08572+3915	4972032	S13.2.0	2004 Apr 15	$31 \times 6 \times 2$	0.0584	12.10	4.2	LINER[1]	258
IRAS 02530+0211	6652160	S13.2.0	2005 Feb 10	$31 \times 3 \times 2$	0.0276	11.04	3.7		119
IRAS 12112+0305	4977664	S13.2.0	2004 Jan 4	$121 \times 2 \times 2$	0.0727	12.33	1.3	LINER[1]	324
IRAS 14348-1447	4981248	S13.2.0	2004 Feb 7	$121 \times 2 \times 2$	0.0827	12.35	2.1	LINER[2]	372
NGC 6240	4985600	S13.2.0	2004 Mar 4	$31 \times 6 \times 2$	0.0245	11.84	1.2	LINER	119

[a] Ramp integration time $\times$ number of cycles $\times$ number of slit positions

[b] Optical/near-IR spectral classifications taken from: (1) (Armus et al., 1989), (2) (Sanders et al., 1988a), (3) (Veilleux et al., 1995), (4) (Low et al., 1988), (5) (Darling & Giovanelli, 2002), (6) (Veilleux et al., 1997)

[c] Assuming $\mathrm{H}_0 = 71\ \mathrm{km\,s^{-1}\,Mpc^{-1}}, \Omega_{\rm M} = 0.27, \Omega_\Lambda = 0.73,$ and $\Omega_{\rm K} = 0$

8.2 Observations

The observations presented in this paper are part of the *Spitzer* IRS observing programs (PID) 105 (IRS GTO ULIRG program, PI: J.R. Houck), 96 (IRS GTO program on nearby AGN, PI: J.R. Houck) and 1096 (Director's Discretionary Time [DDT] proposal, PI: H.W.W. Spoon). The IRS GTO ULIRG sample comprises $\sim$100 ULIRGs in the redshift range $0.02 < z < 0.93$, selected primarily from the IRAS 2 Jy sample (Strauss et al., 1992), IRAS 1 Jy sample (Kim & Sanders, 1998), and the Faint Images of the Radio Sky at Twenty cm (FIRST)/IRAS radio-far-IR sample (Stanford et al., 2000). The samples of PIDs 96 and 1096 contain three additional ULIRGs (IRAS 04384–4848, IRAS 03000–2719, and IRAS 02113–2937) and three additional LIRGs (IRAS 02530+0211, IC 860, and NGC 4418). For all sources in this combined sample, low-resolution spectra ($R = \lambda/\Delta\lambda \sim 100$) have been obtained, while high-resolution spectra ($R = 600$) have been taken only for the brighter half of the sample.

All high-resolution spectra in this sample have been investigated for the presence of vibration-rotation absorption bands of C_2H_2 (13.7 μm), HCN (14.02 μm) and CO_2 (15.0 μm) against the nuclear continuum. Fifteen of the sources listed in Table 8.1 show absorption due to (some of) these species. Because of the low signal-to-noise ratio of the spectra and/or the low H column densities (as derived from the 9.7 μm silicate optical depth; see §8.3.3), the derived upper limits on the molecular column densities for all other sources do not place very stringent constraints on the C_2H_2 and HCN abundances. To illustrate this, four sources without positive detections with both a moderate-to-large hydrogen column density and good signal to noise spectra, are included in Tables 8.1 and 8.2. The upper limits on the C_2H_2 and HCN abundances fall within the range of derived abundances toward the fifteen sources.

Data reduction started from crosstalk corrected echelle images using S12 and S13 *Spitzer* archive data. Processing was done using the Cores to Disks (c2d) analysis pipeline (Kessler-Silacci et al., 2006; Lahuis et al., 2006a, , and Chapter 3). It includes echelle

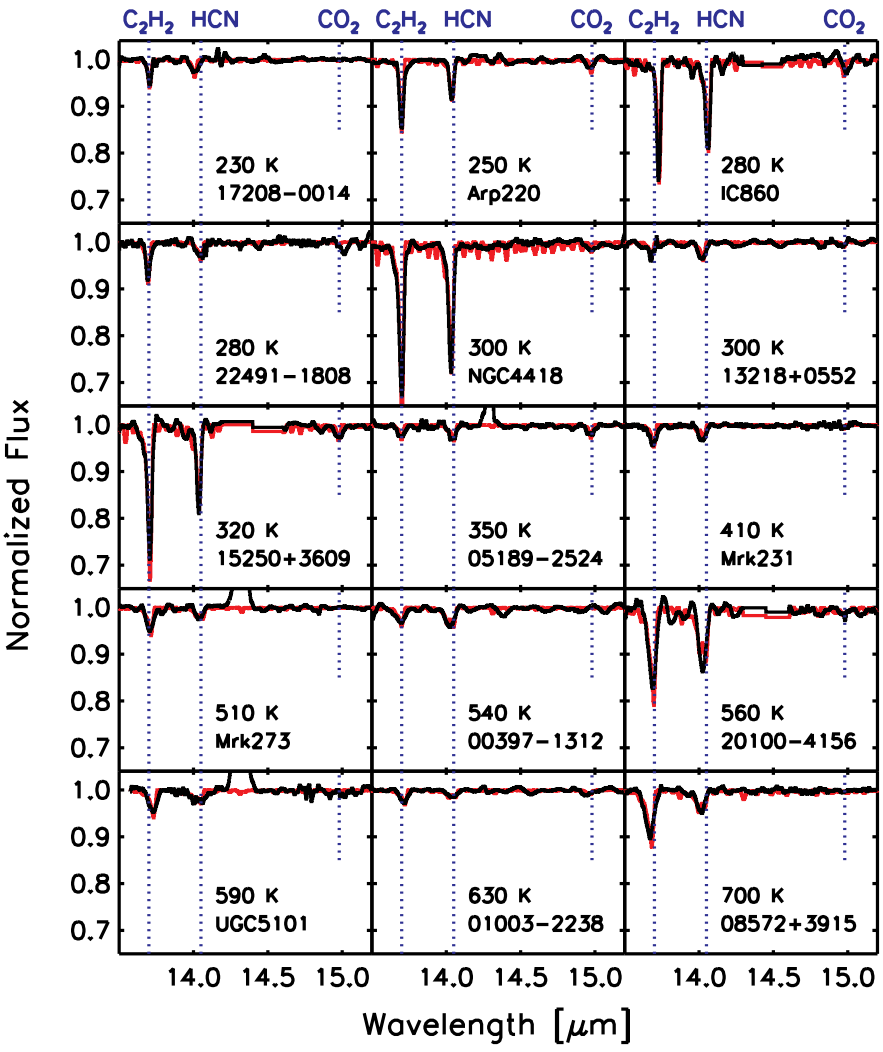

Figure 8.1 Continuum-divided *Spitzer* IRS spectra of a sample of (U)LIRGs showing the absorption bands of C_2H_2 and HCN and some of CO_2. In the ApJ paper and the online thesis the best-fit synthetic spectra, assuming a single excitation temperature for all three molecules, are plotted in red. All spectra have been shifted to the rest wavelengths.

image analysis (among others bad pixel detection, image arithmetic, and optimal spectral extraction), defringing of the extracted spectra (Lahuis & Boogert, 2003), and spectral analysis (see §8.3.1). The optimal spectral extraction uses an analytical source profile defined and calibrated using a suite of calibrator stars. Calibration is done using MARCS stellar models provided by the *Spitzer* Science Center (Decin et al., 2004). The optimal spectral extraction employs a combined source and local sky fit. This provides wavelength-dependent sky estimates and allows discrimination between resolved and unresolved spectral features.

Figure 8.1 shows the continuum-divided, sky, and redshift-corrected spectra from 13.5 to 15.5 μm, covering the absorption bands of C_2H_2, HCN, and CO_2. Plotted in red are the best-fit single temperature synthetic spectra (see §8.3). Indicated with the dotted verticals are the positions of the ground-state Q-branch transitions of the three molecules. For IRAS 15250+3609, IRAS 20100–4156, and IC 860, a small section of the spectrum in between HCN and CO_2 is affected by artifacts in inter-order sections of the spectrum, and these sections have been clipped from the presented spectra.

8.3 Analysis

8.3.1 Molecular analysis

The *Spitzer* spectra unambiguously reveal the presence of the Q-branch transitions of C_2H_2 $\nu_5 = 1 - 0$, HCN $\nu_2 = 1 - 0$, and CO_2 $\nu_2 = 1 - 0$, each of which blends into a "broad" absorption feature. The corresponding P- and R-branch transitions of these species are difficult to observe with the *Spitzer* IRS due to spectral dilution at the IRS resolving power and the presence of instrumental fringe residuals with frequencies and amplitudes close to those of the P- and R-branch lines. The Q-branch transitions are analyzed using a pure absorption model assuming local thermodynamic equilibrium (LTE) excitation of the levels at a single temperature. The adopted method is described in detail in Lahuis & van Dishoeck (2000) and Boonman et al. (2003), which includes references to the molecular parameters and data used in the model. The main fit parameters are the excitation temperature and column density along the line of sight for a given intrinsic line width, defined by the Doppler b-value. It is assumed that the absorbing molecules have a covering factor of unity of the continuum, i.e. the mid-IR continuum is composed solely by the regions toward which the molecular absorption features arise. A covering factor less than unity, i.e. larger continuum emitting regions, increases the true optical depth of the absorption features, resulting in higher column densities and possibly lower temperatures (when lowest excitation lines saturate at large column densities).

The derived excitation parameters do not strongly depend on the exact value of b. Only for low values of b ($\lesssim 5\,\mathrm{km\,s^{-1}}$) will saturation result in an underestimate of the column density for the sources with the largest column densities. Such low b-values are expected for quiescent gas, where thermal broadening dominates. However, non thermal broadening will likely dominate in the dense energetic interstellar medium (ISM) of the galactic nuclei and larger b-values are expected.

A direct estimate of b is obtained from spectrally resolved CO $\nu = 1 - 0$ absorption lines toward the north-west nucleus of IRAS 08572+3915 (Geballe et al., 2006), which shows a complex velocity structure. A low column density, cold CO component absorbs near the systemic velocity. The CO absorption is, however, dominated by a broad (FWHM $\sim 200\,\mathrm{km\,s^{-1}}$) blueshifted warm ($\gtrsim 200$ K) gas component. This is most likely the conglomerate of a velocity distribution over multiple lines of sight within the beam. The continuum confusion then requires a higher column density than that of 2×10^{18} $\mathrm{cm^{-2}}$ estimated from the observed optical depth by Geballe et al. (2006). We have fitted synthetic LTE absorption spectra to the higher excitation CO lines using the spectrum of Geballe et al. (2006), but with the spectral resolution reduced to match the observed profile width ($R \sim 1500$). This allows us to estimate a velocity averaged column density for a given b-value. Values $< 10\,\mathrm{km\,s^{-1}}$ result in progressively poorer fits. Good fits

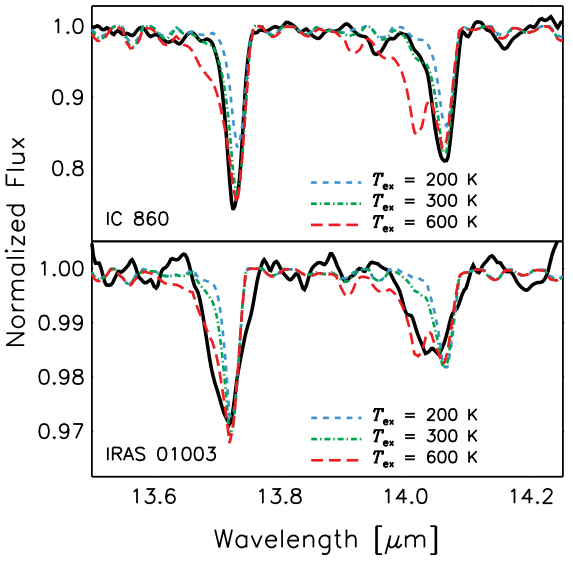

Figure 8.2 Illustration of the temperature sensitivity of the C_2H_2 and HCN Q-branch profiles in direct comparison to the observed spectra of IC 860 (best fit $T_{ex} = 280$ K) and IRAS 01003-2238 (best fit $T_{ex} = 630$ K). The shape of the Q-branch profile determines the derived excitation temperatures with an uncertainty of $\sim 30\%$. A better constrained error estimate is difficult to determine at the IRS resolution.

are made for b-values of $10 - 25\,\mathrm{km\,s^{-1}}$ requiring column densities of $\sim 2 \times 10^{19}$ down to $\sim 5 \times 10^{18}$ cm^{-2}. The Doppler b-value has therefore been fixed to $20\,\mathrm{km\,s^{-1}}$ for all sources.

Recent observations using TEXES (Lacy et al., 2002), a visitor instrument on Gemini-North, have revealed spectrally resolved (FWHM $\sim 80\,\mathrm{km\,s^{-1}}$) blueshifted absorption in the C_2H_2 $\nu_5 = 1 - 0$ $R(13)$ ro-vibrational line toward one of our sources, NGC 4418 (C. Knez 2006, private communication). The current data do not allow us to put more stringent constraints on the Doppler b-value. However, the spectrally resolved C_2H_2 absorption could be an indication that multiple (spatial and velocity) components of the warm and dense gas are common in (U)LIRG nuclei.

8.3.2 Fit results

Table 8.2 lists the derived excitation temperatures and column densities from best fit synthetic spectra to the continuum divided (U)LIRG spectra. Excitation temperatures ranging from 200 to 700 K and column densities of a few 10^{15} to 10^{17} cm^{-2} are observed. These results are derived from a simultaneous fit to the three absorption bands, in which the excitation temperature, set to be the same for all three molecules, is constrained by the Q-branch profiles of C_2H_2 and HCN. Since the analysis is restricted to analysis of the resolved Q-branches (see §8.3.1), the derived excitation temperatures are not well constrained ($\sim 30\%$). However, it does clearly allow us to discriminate between molecular gas with warm ($\sim 200 - 300$ K) and hot ($\sim 500 - 700$ K) excitation temperatures. This is illustrated in Figure 8.2 by fits to the observed absorption profiles of IC 860 and IRAS 01003-2238, for which we derive excitation temperatures of 280 and 630 K, respectively.

The Q-branch profiles of C_2H_2 and HCN reveal significant contributions to the absorption from relatively high rotational levels. Hence, given the high critical density of these levels, the absorbing gas is likely very dense ($n \gtrsim 10^7$ cm^{-3}). Observations of

Table 8.2. LTE excitation parameters and spectral characteristics

Target	$T_{\rm ex}$ [a]	$N_{\rm C_2H_2}$ [a]	$N_{\rm HCN}$ [a]	$N_{\rm CO_2}$ [a]	$N_{\rm H_2}$	$x_{\rm C_2H_2}$ [b]	$x_{\rm HCN}$ [b]	$x_{\rm CO_2}$ [b]	cont.[c]	S/N[d]
		10^{16}	10^{16}	10^{16}	10^{22}	10^{-8}	10^{-8}	10^{-8}		
	(K)	($\rm cm^{-2}$)	($\rm cm^{-2}$)	($\rm cm^{-2}$)	($\rm cm^{-2}$)				(Jy)	
17208-0014	230	0.6	1.2	< 0.2	3.3	18	36	< 6	0.20	200
Arp 220	250	1.7	2.9	0.7	5.8	29	50	12	0.93	150
IC 860	280	3.1	7.2	0.9	3.7	84	195	24	0.09	150
22491-1808	280	1.0	1.4	< 0.3	1.9	53	74	< 16	0.07	130
NGC 4418	300	5.3	12.	< 0.4	7.7	69	156	< 5	2.34	150
13218+0552	300	0.4	1.5	< 0.5	1.4	28	107	< 36	0.26	180
15250+3609	320	4.7	7.0	0.7	6.7	70	105	10	0.27	90
05189-2524	350	0.4	1.5	0.8	0.7	57	214	114	1.05	200
Mrk 231	410	0.6	1.4	< 0.4	1.4	43	100	< 29	2.83	200
Mrk 273	510	0.9	1.7	< 0.4	3.3	27	52	< 12	0.37	200
00397-1312	540	0.6	3.0	< 0.4	5.8	10	52	< 7	0.12	150
20100-4156	560	3.8	8.9	< 0.9	5.8	66	153	< 15	0.11	70
UGC 5101	590	1.0	2.2	< 0.5	3.0	33	73	< 17	0.24	130
01003-2238	630	0.5	1.3	< 0.8	1.2	42	108	< 67	0.27	200
08572+3915	700	2.4	3.7	< 0.5	7.4	32	50	< 7	0.74	150
02530+0211	300[e]	< 0.5	< 3	< 0.3	6.5	< 8	< 46	< 5	0.25	100
12112+0305	300[e]	< 0.8	< 2.3	< 0.6	3.0	< 27	< 77	< 20	0.07	150
14348-1447	300[e]	< 0.5	< 1	< 0.2	3.7	< 14	< 27	< 5	0.07	80
NGC 6240	300[e]	< 0.2	< 0.7	< 0.6	2.1	< 10	< 33	< 29	0.68	100

[a] The excitation temperature is poorly constrained and can be uncertain up to 30%. See §8.3.2 and Figure 8.2 for details.

[b] Abundances with respect to $\rm H_2$ assuming $N_{\rm H} = \tau_{9.7}(3.5 \times 10^{22})\ \rm cm^{-2}$ and $N_{\rm H} = 2 \times N_{\rm H_2}$ (see §8.3.3).

[c] Continuum at 14 μm in the rest wavelength frame.

[d] Signal-to-noise ratio (S/N) estimated from the residuals after subtraction of the synthetic spectrum. It varies over the covered wavelength range.

[e] Temperature fixed to 300 K for derivation of column density upper limit estimates.

the ro-vibrational transitions of CO in IRAS 08572+3915 and IRAS 00183-7111 indeed imply densities in excess of 3×10^6 cm^{-3} (Geballe et al., 2006; Spoon et al., 2004).

8.3.3 Abundances

The derived column densities are translated into abundances by using a total hydrogen column density obtained from the apparent optical depth of the 9.7μm silicate absorption band listed in Table 8.1. The optical depth is converted assuming

$$N_{\rm H} = \tau_{9.7}(3.5 \times 10^{22})\,{\rm cm}^{-2}$$

appropriate for the dust in the solar neighbourhood (Roche & Aitken, 1984, 1985).

This relation is most appropriate for embedded (extinction dominated) sources when probing the absorption along the pencil beam line of sight toward the warm central continuum emitting region. To illustrate, for the sample of Galactic massive protostars (see §8.4.3), the hydrogen column density derived using the silicate optical depth estimated from the ISO-SWS archive spectra agrees within a factor of two with the hydrogen column density derived from CO $\nu = 1 - 0$ measurements (Mitchell et al., 1990; Lahuis & van Dishoeck, 2000).

Another estimate of the applicability of this method is provided through the analysis of the 4.6 μm CO $\nu = 1 - 0$ absorption spectrum toward the source IRAS 08572+3915 NW, which gives CO column densities of $\sim 5 \times 10^{18}$ up to $\sim 2 \times 10^{19}\,{\rm cm}^{-2}$, depending on the assumed value of b (see §8.3.1). Adopting $N_{\rm CO}/N_{\rm H} = 10^{-4}$ (all gas-phase carbon in CO), this results in $N_{\rm H} = 5 \times 10^{22}$ to $2 \times 10^{23}\,{\rm cm}^{-2}$. This is in reasonable agreement with the hydrogen column density derived from the silicate optical depth ($N_{\rm H} \sim 1.5 \times 10^{23}\,{\rm cm}^{-2}$). If anything, the IRAS 08572+3915 NW data suggest the hydrogen column density might be slightly overestimated (e.g. as a result of foreground

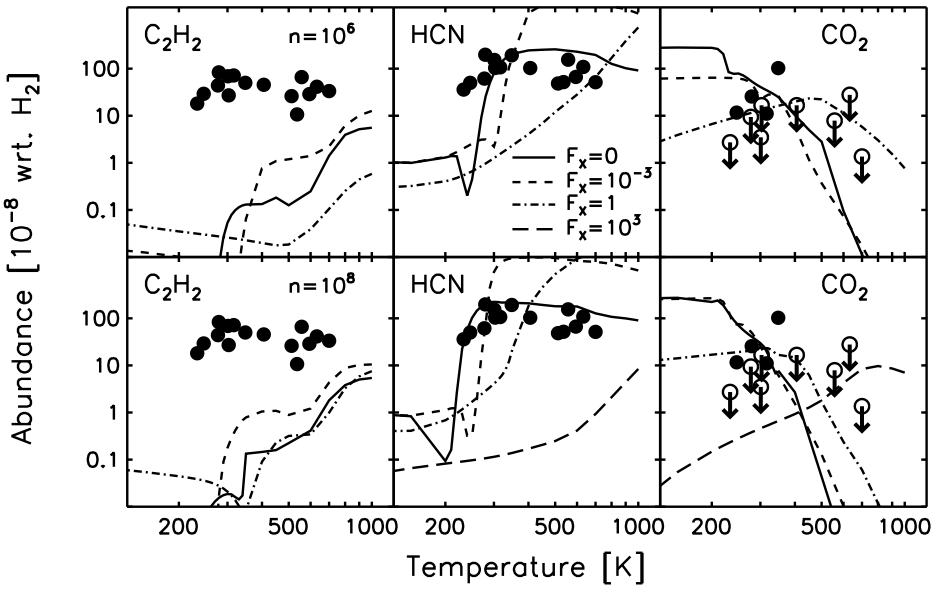

Figure 8.3 Results of equilibrium X-ray-enhanced chemical models for the three observed molecules. The calculated abundances are shown for moderate ($10^6\,\mathrm{cm}^{-3}$) and high density ($10^8\,\mathrm{cm}^{-3}$) and for four X-ray flux levels ($F_\mathrm{X} = 0$, 10^{-3}, 1 and 10^3 erg cm^{-2} s^{-1} plotted with solid, dashed, dot-dashed, and long-dashed lines, respectively). Note that except for HCN and CO_2 at high density, the abundances for the highest X-ray flux are below the plotted range. Overplotted are the observed abundances. Details of the model can be found in Stäuber et al. (2005); Stauber et al. (2006).

extinction) resulting in underestimating the derived molecular abundances. We assume a similar uncertainty for the other sources.

The derived abundances and H_2 column densities (assuming $N_{\mathrm{H}_2} = N_\mathrm{H}/2$) are listed in Table 8.2. The HCN abundance is up to three orders of magnitude higher than in cold molecular clouds (Bergin & Langer, 1997). High abundances of HCN, C_2H_2, and CO_2 have also been measured for Galactic massive protostars (see §8.4.3). Figures 8.3 and 8.4 compare the abundances to chemical models and results from studies of Galactic massive young stellar objects (§8.4).

8.3.4 Gas temperature

The derived excitation temperatures range from 200 to 700 K. While statistics are small, of the seven sources with the highest gas excitation temperatures ($T_{ex} = 400 - 700\,\mathrm{K}$), five sources show the highest $5.5 - 28\,\mu$m continuum flux ratio. These galaxies also show a rising near-IR continuum typical for hot dust while the other galaxies show a decreasing near-IR continuum characteristic for emission dominated by stellar photospheres. It seems thus that there is a connection between the observed dust and molecular excitation temperatures.

The presence of absorption (rather than emission) lines implies a strong gradient in the temperature and an underlying hot-dust continuum against which the absorption

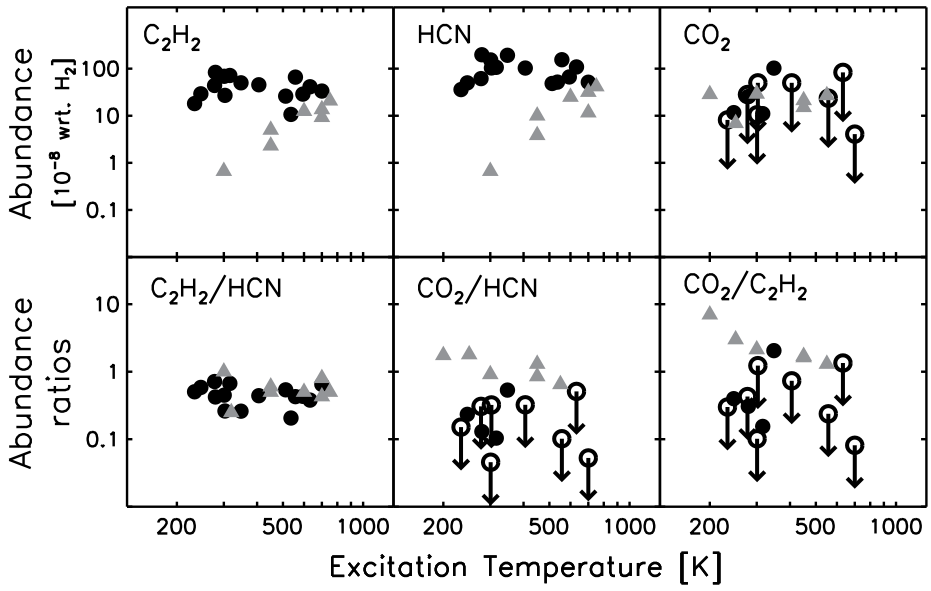

Figure 8.4 *Top:* Observed C_2H_2, HCN, and CO_2 abundances using a total H_2 column obtained from the $9.8\,\mu$m silicate absorption band. *Bottom:* Abundance ratios of C_2H_2, HCN and CO_2. Both the absolute abundances and the abundance ratios are indicated with circles and are presented as functions of excitation temperature. Included are the observed values toward a sample of Galactic massive YSOs (Boonman et al., 2003; Lahuis & van Dishoeck, 2000) plotted with grey triangles. The derived absolute abundances toward the (U)LIRGs show significant enhancements in the abundances of C_2H_2 and HCN for sources with excitation temperatures below 500 K. The C_2H_2/HCN abundance ratios are quite similar however, the CO_2/C_2H_2 and CO_2/HCN ratios toward the (U)LIRGs are systematically lower than toward the Galactic massive YSOs, suggesting that a different chemistry may apply.

lines are formed. However, the derived excitation temperatures of the molecular gas for the warmest sources ($T_{ex} = 400 - 700$ K) are higher by a factor of $2 - 3$ than the mid-IR color temperature derived from the $5.5 - 28.0\,\mu$m flux ratio. While the discrepancy between the excitation temperatures and the mid-IR color temperature may (in part) reflect the uncertainties in the analysis, the observed colder dust continuum may point towards the importance of continuum extinction by (a shell of) colder foreground dust exterior to the C_2H_2 and HCN absorbing layer, or the predominance of emission of cold nuclear dust within the IRS aperture (i.e. a small beam filling factor for the warm dust and gas). Both may result in an added uncertainty in the derived abundances resulting from overestimating the hydrogen column density or from a covering factor of the molecule rich warm gas less than unity (see §8.3.1).

8.4 Discussion

8.4.1 Warm molecular gas in (U)LIRGs

The *Spitzer* IRS spectra reported here reveal surprisingly strong mid-IR absorption bands of C_2H_2, HCN, and CO_2 toward a sample of (U)LIRG nuclei. These absorptions reveal the presence of copious amounts of warm molecular material and are in line with earlier detections of warm CO gas (Spoon et al., 2004, 2006; Geballe et al., 2006). This molecular gas is very dense ($n \gtrsim 3 \times 10^6$ cm^{-3}) and warm ($T \sim 200 - 700$ K). Given the column density and estimated density, this gas occupies only a small fraction of the nuclear region (~ 0.01 pc) and, given its high temperature, is likely located near the intrinsic mid-infrared source of luminosity of these regions.

At present there are still substantial uncertainties in accurately inferring the nature of the power source dominating the bolometric luminosity in infrared luminous galaxies. As discussed in Armus et al. (2007), it appears that there are disagreements among various diagnostic diagrams based on line ratios, continuum colors or PAH equivalent width. Perusal of the $2 - 40\mu$m spectra reveal that the sources with molecular gas absorptions appear to be a "mixed bag." While most sources show a deep silicate feature, some (e.g., Mrk 231, IRAS 01003-2238, IRAS 05189-2524, and IRAS 13218+0552) do not. Indeed, the $2 - 40\mu$m continuum spectra of these sources show strong similarities with the spectra of bona fide AGN-dominated spectra with shallow silicate features. In contrast, sources like IRAS 17208-0014 and IRAS 22491-1808 look quite starburst-like. Finally, sources such as IRAS 08572+3915 show neither signs of starburst activity (e.g., PAH features) nor signs of AGN activity (e.g., high ionization lines or a broad Hα line). While the presence of hot dust, as visible in the near-IR, may be taken as evidence for the presence of an embedded AGN in this source, any deeply obscured source, including deeply embedded protostars, will produce hot dust. Indeed, the overall mid-IR spectrum of IRAS 08572+3915 resembles that of many galactic massive protostars, such as AFGL 2591, with a preponderance of dust absorption features.

The C_2H_2, HCN, and CO_2 molecular lines may provide a new probe of the conditions in the inner deeply obscured nuclei and hence shed light on the ultimate power source of (U)LIRGs; e.g., starburst phenomena versus AGN activity. In particular, the presence of copious amounts of warm molecular gas enriched in C_2H_2, HCN, and CO_2 is common in regions of massive star formation (Boonman et al., 2003; Lahuis & van Dishoeck, 2000; Lacy et al., 1989; Evans et al., 1991), while, on the other hand, X-rays associated with a central black hole can influence molecular chemistry and abundances far beyond the mean free path length of stellar (E)UV photons. The molecular observations are discussed in the light of these scenarios in §§8.4.2, 8.4.4, and 8.4.3. While the possible errors associated with the derived abundances are recognized, the discussion will center on Figures 8.3 and 8.4.

8.4.2 AGN activity and X-ray-driven chemistry

Submillimeter studies have revealed high HCN/CO (and HCN/HCO$^+$) abundance ratios in Seyfert type I nuclei, and this has been taken as an indication of the importance of X-ray illumination for the composition of the molecular gas in these nuclei (Imanishi et al., 2006; Kohno, 2005). Some of the sources in our sample are known to harbor an AGN. In particular, Mrk 231 and IRAS 13218+0552 are QSOs; IRAS 08572+3915 and

UGC 5101 are LINERs; and IRAS 01003-2238, IRAS 05189-2524, and Mrk 273 have optical LINER/Seyfert 2 spectra (see Table 8.1). Hence, the observed high abundance of HCN, and by inference of C_2H_2 (which has no pure rotational transitions), may indicate the presence of a buried AGN in all of our sources. The complex geometry and inhomogeneous dust distribution associated with the central toroid may then preclude our detection of the putative X-rays photons from the central engine driving the chemistry of the molecular gas. The mid-IR observations presented in this paper add to the submillimeter results the predominance of *warm* molecular gas. Within the AGN heating scenario, it seems obvious to attribute the high temperature of the molecular gas to the importance of X-ray heating in a so-called X-ray dominated region (XDR, Maloney et al., 1996; Meijerink & Spaans, 2005). Alternatively, Gao & Solomon (2004) argue that most (U)LIRGs are dominated by starburst power rather than AGN power, based on the HCN $J = 1 - 0$ luminosity and CO $J = 1 - 0$ luminosity relation. In a starburst scenario, the HCN/CO ratio traces the amount of dense molecular gas in the galactic ISM. Our observations may present an additional test for these two scenarios.

X-rays are not only an efficient heating agent of the gas, but also have a major influence on the chemical composition. This has been explored in the context of AGNs by Maloney et al. (1996); Meijerink & Spaans (2005), and for regions around protostars by Stäuber et al. (2005); Stauber et al. (2006). At the high densities relevant for these regions, the gas temperature is set by a balance between X-ray heating and gas-dust collisional cooling. As an example, a gas temperature of 200 K at a density of $\sim 3 \times 10^6$ cm^{-3} requires a X-ray flux of $\sim$ 30 erg cm^{-2} s^{-1}, which for a typical Seyfert galaxy with an X-ray luminosity of 10^{44} erg s^{-1} corresponds to a distance of 50 pc for an unobscured view of the central engine. For the molecular features to be seen in absorption, the mid-IR continuum has to arise from an inner, warmer zone (e.g., exposed to a higher X-ray flux). Since most of these (U)LIRGs show no evidence for strong X-ray emission while the column density associated with the molecular gas ($10^{22} - 10^{23}$ cm^{-2}) is small compared to X-ray attenuation lengths, in this AGN scenario, the direct view of the nucleus would have to be blocked by a high column density, edge-on toroid, while the warm molecular gas is offset to the polar regions and has a little-obstructed view of the nucleus.

An AGN origin for the high abundance of warm HCN, C_2H_2, and CO_2 in these (U)LIRGs, however, faces severe theoretical difficulties. Specifically, the high X-ray flux required to explain the observed temperatures readily dissociates the molecules and drives the gas atomic (Maloney et al., 1996; Meijerink & Spaans, 2005). Indeed, calculated HCN abundances are typically less than 10^{-8} with respect to H in X-ray illuminated gas, while C_2H_2 is virtually destroyed for X-ray fluxes in excess of 1 erg cm^{-2} s^{-1}. This is illustrated in Figure 8.3, which presents the static steady state chemical composition after equilibrium is reached ($\sim 10^5$ yr) for clouds illuminated by X-rays. Here, "static" means that the chemistry has been evolved in time while the X-ray flux, temperature, and density are fixed until steady state is achieved in the chemical abundances (see also Stäuber et al., 2005; Stauber et al., 2006). The X-ray spectrum is assumed to be thermal in nature, with $T_{\rm X}$=3 $\times$ 10^7 K. The chemistry is relatively insensitive to the assumed shape of the spectrum (e.g., Maloney et al., 1996). As these models demonstrate, strong X-ray irradiation leads to decreased abundances of molecular species such as HCN and C_2H_2. These results are consistent with earlier studies (e.g., Lepp & Dalgarno, 1996), which show an initial increase in the HCN abundance

with increasing ionization rate ($\xi/n_{\rm H}$ up to $10^{-18}\,{\rm cm}^{-3}\,{\rm s}^{-1}$) but then an effectively complete destruction of HCN for $\xi/n_{\rm H} \gtrsim 10^{-17}\,{\rm cm}^{-3}\,{\rm s}^{-1}$. For comparison, the X-ray flux implied by a gas temperature of 200 K ($\simeq 30$ erg cm^{-2} s^{-1}) corresponds to an ionization rate of 5×10^{-17} cm^{-3} s^{-1} at a density of 10^6 cm^{-3}. Clearly, the warm molecular gas revealed by these observations is inconsistent with strong X-ray illumination.

8.4.3 Static hot-core chemistry

At first sight our mid-infrared results resemble those toward a sample of massive Galactic young stellar objects (YSOs). For these, the molecular absorption features originate in the warm, dense gas near the newly formed star during the so-called hot core phase (Boonman et al., 2003; Lahuis & van Dishoeck, 2000; Lacy et al., 1989; Evans et al., 1991). This is generally thought to represent a very early phase ($\Delta t \leq 10^5$ yr) in the formation of massive stars, during the transition from the deeply embedded stage to the phase where ionizing photons can escape the protostellar accretion envelope and create first a hyper- and later an ultra-compact HII region (see review by Cesaroni, 2005a). The molecular composition of the hot core is very different from that of cold molecular clouds. This is thought to reflect the evaporation of ices, resulting from accretion and surface chemistry during the cold preceding dark cloud phase, when the envelope is heated by the newly formed star (Walmsley & Schilke, 1993). Subsequent high temperature gas-phase chemistry significantly enhances the abundance of e.g. CH_4, C_2H_2, and HCN up to three orders of magnitude, compared to cold dense molecular cloud abundances, for the most evolved sources (Viti & Williams, 1999; Doty et al., 2002; Rodgers & Charnley, 2003).

In Figure 8.4 the observed abundances and abundance ratios toward the (U)LIRGs are compared to those of a sample of Galactic massive YSOs. Both the YSO and the (U)LIRG sample show comparable, large variations in gas temperature and abundances. However, the HCN and C_2H_2 abundances show a positive correlation with the gas temperature for the YSO sample but not for the (U)LIRG sample. Indeed, at low temperatures (< 400 K), the (U)LIRG abundances are some two orders of magnitude larger than those in YSO spectra.

For the Galactic YSOs, the observed correlation between the excitation temperature and the observed abundances (Fig. 8.4) are in fair agreement with chemical models for such regions (Stäuber et al., 2005). The absence of a similar temperature correlation for (U)LIRGs may reflect a systematic (and large) error in the abundance determination (§8.3.3) or it may reflect a true difference between the chemical or physical evolution of the warm gas of the YSOs and (U)LIRGs. In this respect, we note that the C_2H_2/HCN ratios for both samples are very similar; however, the CO_2/HCN and CO_2/C_2H_2 ratios are reduced for the (U)LIRG sample up to an order of magnitude. If static steady state hot-core chemistry were to apply to the (U)LIRGs as it does to the YSOs, CO_2 would have been detected toward most of the sources in our sample. The fact that it has not suggests that a different chemistry may apply to the warm molecular gas in these (U)LIRGs.

8.4.4 Pressure confined starburst chemistry

Static steady state hot-core and X-ray chemical models have difficulties consistently reproducing the observed high abundances of warm C_2H_2 and HCN gas and low abun-

dance of CO_2 gas for most of our (U)LIRG sample. Essentially, static chemistry has a hard time producing high abundance of HCN and C_2H_2 in the warm ($100 - 400$ K) gas characteristic for most of our (U)LIRG sample, while at the same time reducing the CO_2 abundance. One possible solution to this conundrum is to produce high C_2H_2 and HCN, and low CO_2 abundances in hot gas ($\gtrsim 800$ K), and then transport it outward to the cooler gas on a dynamical timescale that is rapid compared to the chemical timescale. At high temperatures, the hydrocarbon and nitrogen chemistries are enhanced, as most of the oxygen is converted into water by neutral-neutral reactions. The abundances of molecules such as C_2H_2, CH_4, and HCN can be increased by orders of magnitude (e.g., Doty et al., 2002; Rodgers & Charnley, 2003) while at the same time the formation of CO_2 is reduced as its primary formation route through OH is blocked. For cold Galactic molecular clouds, the chemical timescale is set by the cosmic ray ionization rate and is about 3×10^5 yr, independent of density (Glassgold & Langer, 1973). In a (U)LIRG (or AGN) environment, the cosmic ray flux may be increased considerably, shortening this timescale. Likewise, neutral-neutral reaction channels may open up in warm gas, further reducing the chemical timescale. In any case, these timescales are much shorter than the evolutionary timescale of massive stars or of the starburst. With the typical sizescale of the warm molecular zone ($\sim 3 \times 10^{16}$ cm), a timescale of 3×10^5 yr translates into a 'diffusion' velocity of only 0.03 km s^{-1}. Even a 100 times faster chemical timescale only requires a 'diffusion' velocity of a few km s^{-1}. Since the chemical models are well capable of explaining high abundances for both C_2H_2 and HCN and a low abundance for CO_2 at high temperatures and densities, and in light of the discussion above, this "mixing" is attributed to the global activity created by pressure-confined massive starburst activity. The strong gravitational potential in the nuclei of these galaxies inhibits the disruption of the surrounding warm molecular envelopes by H II regions and supernovae, while producing sufficient turbulent (or wind) motion to distribute warm C_2H_2- and HCN-rich and CO_2-poor gas in the colder outer envelope regions.

8.5 Summary

We have observed the absorption lines due to the Q-branch transitions of C_2H_2, HCN, and CO_2 in the mid-IR spectra of a large number of (U)LIRGs. These observations reveal for the first time the presence of copious amounts of warm (200-700 K), dense ($n > 10^7$ cm^{-3}) molecular gas in these nuclei. The origin of this warm molecular gas is unclear. Theoretical models show that the X-ray fluxes implied by the elevated gas temperatures rapidly destroy these molecules, and hence it is unlikely that this warm molecular gas is associated with a dense toroid surrounding an active central engine. Warm, dense gas rich in C_2H_2, HCN, and CO_2 is commonly observed towards galactic massive protostars and is associated with a short-lived phase, the hot-core phase, before advancing ionization fronts disrupt the core. The high molecular abundances in galactic hot-cores are well understood chemically. However, the derived abundances of C_2H_2 and HCN for the cooler (U)LIRGs ($T_{\rm ex} \simeq 200 - 400$ K) in our sample as well as the C_2H_2/CO_2 and HCN/CO_2 ratios are very different from those in galactic protostars. We suggest that this warm molecular gas is associated with a phase of deeply embedded star formation in (U)LIRGs, where the high pressures and densities have inhibited the disruption of the star forming, molecular cores by prohibiting the expansion of H II regions, trapping the star formation process in an extended hot-core phase. The

chemical differences between these (U)LIRGs and galactic hot-cores may then reflect enhanced mixing between warm and cold phases due to the high degree of turbulence or wind motion associated with extreme starburst environments. Pressure-confined massive starburst activity may thus be the driving energy source behind the observed C_2H_2 and HCN rich warm molecular gas and be responsible for most of the near-IR characteristics of the deeply obscured (U)LIRGs.

The current analysis is predominately based on the observed abundances derived from moderate resolution, mid-IR vibration-rotation absorption bands of C_2H_2 and HCN. This analysis can be extended using high-resolution, velocity resolved, ground-based studies of the P- and R-branches of these molecules, as well as from the $\nu = 1-0$ rotation-vibration band of CO. In addition, observations of more molecular rotation-vibration bands and high-excitation submillimeter lines of a large sample of molecules may be instrumental for progress in this field. Specifically, velocity and spatially resolved infrared and millimeter data can constrain the source morphology. In combination with optimized physico-chemical models for individual sources, it may become possible to draw firm conclusions about the physical characteristics of the warm molecular gas and the true nature of the power sources in the (U)LIRG nuclei.

Acknowledgements

The authors would like to thank Tom Geballe for sharing early results and the CO data of IRAS 08572+3915 NW; John Lacy and Claudia Knez for sharing the TEXES data; and Bernhard Brandl, Kees Dullemond, Masa Imanishi, David Rupke, and Marco Spaans for many useful discussions. Astrochemistry in Leiden is supported by a Spinoza grant from NWO.